Tellus SERIES B CHEMICAL AND PHYSICAL METEOROLOGY
PUBLISHED BY THE INTERNATIONAL METEOROLOGICAL INSTITUTE IN STOCKHOLM

Tellus (2011), 63B, 800–813
Printed in Singapore. All rights reserved

TELLUS

Regional modelling of Saharan dust and biomass-burning smoke

Part 2: Direct radiative forcing and atmospheric dynamic response

By BERND HEINOLD[1,2]*, INA TEGEN[1], STEFAN BAUER[3] and MANFRED WENDISCH[3],
[1]*Leibniz Institute for Tropospheric Research, 04318 Leipzig, Germany;* [2]*School of Earth and Environment, University of Leeds, Leeds LS2 9JT, UK;* [3]*Leipzig Institute for Meteorology, University of Leipzig, 04103 Leipzig, Germany*

(Manuscript received 10 November 2010; in final form 14 June 2011)

ABSTRACT

The direct radiative forcing and dynamic atmospheric response due to Saharan dust and biomass-burning aerosol particles are presented for a case study during the SAMUM-2 field campaign in January and February 2008. The regional model system COSMO-MUSCAT is used. It allows online interaction of the computed dust and smoke load with the solar and terrestrial radiation and with the model dynamics. Model results of upward solar irradiances are evaluated against airborne radiation measurements in the Cape Verde region. The comparison shows a good agreement for the case of dust and smoke mixture. Dust and smoke particles influence the atmospheric dynamics by changing the radiative heating rates. The related pressure perturbations modify local and synoptic scale air-flow patterns. In the radiative feedback simulations, the Hadley circulation is enhanced and convergence zones occur along the Guinea coast. Thus, the smoke particles spread more than 5° further north and the equatorward transport is reduced. Within the convergence zones, Saharan dust and biomass-burning material are more effectively advected towards the Cape Verdes. Given the model uncertainties, the agreement between the modelled and observed aerosol distribution is locally improved when aerosol–radiation interaction is considered.

1. Introduction

This contribution is the companion publication to Heinold et al. (2011), who present regional transport simulations of Saharan dust and biomass-burning aerosol during the second field campaign of the Saharan Mineral Dust Experiment (SAMUM-2). The model includes simulations of the interaction of the computed aerosol load with the solar and terrestrial radiation and with the atmospheric dynamics. Here, we study the direct aerosol radiative forcing and dynamic atmospheric response due to dust and vegetation-fire smoke particles on the basis of those regional model simulations.

Desert dust and biomass-burning particles influence the radiation budget of the Earth-atmosphere system by scattering and absorption of incoming solar radiation as well as absorption and re-emission of outgoing terrestrial radiation (e.g. Sokolik and Toon, 1996; Haywood and Boucher, 2000; Myhre et al., 2003, 2008; Malavelle et al., 2011). The presence of mineral dust and smoke particles reduces the surface heat and moisture fluxes and changes atmospheric heating rates (e.g. Ramanathan et al., 2001; Yu et al., 2002). As a result, the atmospheric stability, local and large-scale atmospheric circulations as well as the hydrological cycle are modified. The response of the boundary layer dynamics to the dust forcing can affect the emission of mineral dust itself (Miller et al., 2004; Pérez et al., 2006; Heinold et al., 2008). Moreover, the direct radiative impact of Saharan dust has the potential to change the dynamics of the West African monsoon and precipitation patterns (e.g. Yoshioka et al., 2007; Solmon et al., 2008; Lau et al., 2009; Zhao et al., 2010). With respect to the radiative effects and feedbacks of biomass burning aerosol particles, several recent studies report on changes in the atmospheric dynamics and convective precipitation in Amazonia as well as over the tropics from the Pacific and Indian Ocean to the Atlantic Ocean (e.g. Wang, 2007; Zhang et al., 2009).

Major sources of mineral dust and vegetation-fire smoke are situated on the African continent. The Sahara desert and the Sahelian region are the most important contributors to the global dust emissions (Washington et al., 2003). During Northern Hemisphere winter, the transport of Saharan dust takes place

*Corresponding author.
e-mail: b.heinold@leeds.ac.uk
DOI: 10.1111/j.1600-0889.2011.00574.x

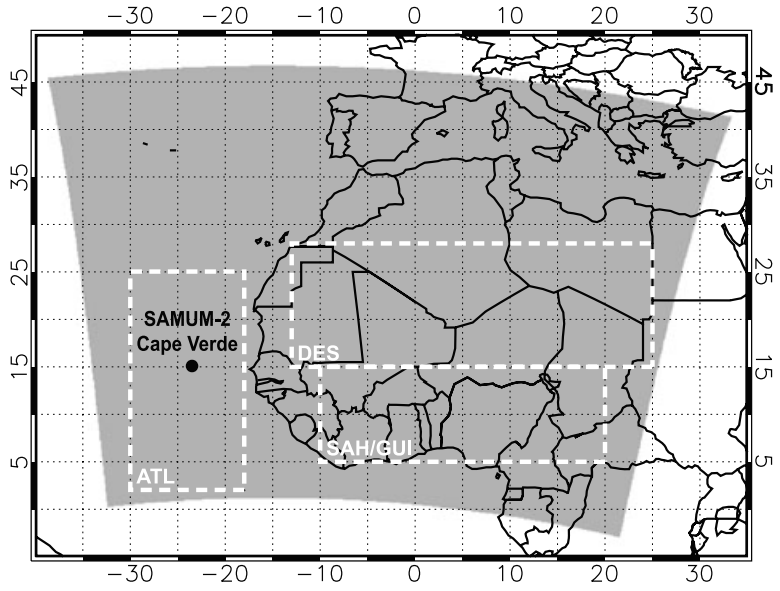

Fig. 1. The model domain for the SAMUM-2 simulations and the location of the observation site Praia, Cape Verde. White dashed boxes indicate the regions over which the dust and smoke optical properties are averaged: Saharan desert (DES: 15°N–28°N; 13°W–25°E), Sahel/Guinea Coast (SAH/GUI: 5°N–15°N; 10°W–20°E) and tropical Atlantic Ocean (ATL: 2°N–25°N; 18°W–30°W).

in shallow surface-near layers and is mainly directed off the West African continent towards Central and South America (Kalu, 1979; Kaufman et al., 2005; Schepanski et al., 2009). A complex aerosol layer structure often forms over West Africa and the adjacent tropical Atlantic Ocean when the dust layers merge with plumes from the widespread biomass-burning activities in southern West Africa, which peak during winter dry season (e.g. Barbosa et al., 1999; Andreae and Merlet, 2001; Haywood et al., 2008; van der Werf et al., 2010).

The mixed plume of Saharan dust and biomass burning aerosol was subject of the second phase of SAMUM. Comprehensive remote sensing and in situ measurements were taken during the field campaign on the Cape Verde Islands in January and February 2008 to investigate the vertical aerosol layering and radiative effects (Ansmann et al., 2011). Within SAMUM-2 we developed and applied a regional coupled dynamic and radiation model for simulations of the dust and smoke plume and its radiative effects (Heinold et al., 2011). This paper presents a detailed study on the direct aerosol radiative forcing and dynamic atmospheric response due to dust and vegetation-fire smoke particles. We make use of the regional model results that were described and thoroughly evaluated in Heinold et al. (2011). Particular focus is on radiative impacts on regional circulation patterns and implications for the aerosol transport itself. In addition, modelled irradiances and airborne radiation measurements obtained within SAMUM-2 are compared in order to quantify the solar radiative impact of Sahara dust partly mixed with biomass-burning particles.

2. Model description and experimental setup

2.1. Regional model COSMO-MUSCAT

The regional model system COSMO-MUSCAT is used to simulate the transport and radiative effects of Saharan dust and biomass burning aerosol particles during SAMUM-2. A detailed model description is given in Heinold et al. (2011). So, here only the main features are briefly summarized. The model components are the non-hydrostatic dynamic model COSMO (Steppeler et al., 2003) and the coupled three-dimensional MUltiScale Chemistry Aerosol Transport Model (MUSCAT) (Wolke et al., 2004; Renner and Wolke, 2010). The model system includes parametrizations for emissions of soil–dust and biomass-burning particles. Dust emission and transport are computed on the basis of meteorological and hydrological fields from COSMO. The model takes into account the spatial–temporal evolution of the dust size distribution, which is parametrized by five independent size bins with radius limits at 0.1, 0.3, 0.9, 2.6, 8 and 24 μm. Biomass-burning emissions are prescribed from satellite fire products. The vegetation-fire smoke is composed of particles with diameters smaller than 2.5 μm (PM2.5). Dry and wet depositions are the processes that remove dust and smoke particles from the atmosphere.

For the SAMUM-2 simulations, a horizontal grid resolution of 28 km is used. The vertical grid has 40 layers from surface to tropopause with a first-layer depth of about 68 m. The model domain includes relevant Saharan dust emission areas, West African vegetation fires and the eastern Tropical Atlantic Ocean (Fig. 1). The dust and smoke radiative effects are investigated for the days 25 January to 7 February 2008, even though the transport simulations are performed for the entire period from 10 January to 7 February. Initialization and large-scale meteorological forcing of COSMO-MUSCAT are based on 6-hourly analyses from the global model GME (Majewski et al., 2002) of the German weather service (Deutscher Wetterdienst, DWD). To prevent long-term drifts in the modelled meteorology, the model system is reinitialized every 48 h using aerosol concentrations at the end of each run to initialize the follow-up cycle.

2.2. Aerosol radiative feedback

The regional model system accounts for aerosol–radiation interactions (Helmert et al., 2007). Solar and thermal radiative fluxes are computed online with the modified COSMO radiation scheme (Ritter and Geleyn, 1992), considering variations in the modelled size-resolved aerosol fields. The radiation effects can influence the COSMO meteorology and feed back on dust emission and aerosol transport.

For the aerosol radiative feedback simulations, the wavelength-dependent dust optical thickness $\tau(\lambda)$ is calculated from the modelled atmospheric mass loads of mineral dust according to

$$\tau(\lambda) = \frac{3}{4} \sum_j \frac{Q_{\text{ext}}(\lambda,\, r_{\text{eff}}(j))}{r_{\text{eff}}(j)\, \rho_{\text{dust}}} M_{\text{dust}}(j)\,, \tag{1}$$

where $Q_{\text{ext}}(\lambda,\ j)$ is the dimensionless particle extinction efficiency of the dust mode j at wavelength λ. $r_{\text{eff}}(j)$ is the effective radius, ρ_{dust} denotes the dust particle density and $M_{\text{dust}}(j)$ the mass load of dust. The spectral optical properties are calculated for each bin from Mie theory using the refractive indices from laboratory measurements reported by Sokolik and Toon (1999). An internal mixture of 98% kaolinite and 2% haematite is assumed. For example for dust particles of 1.5 μm effective radius, the single scattering albedo is 0.79 at 250–700 nm and 0.98 at 700–1530 nm (Helmert et al., 2007, Table 1). Accordingly, at $\lambda = 550$ nm Q_{ext} in eq. (1) is 1.684 for the smallest dust bin, 3.165, 2.352, 2.145 and 2.071 for the larger bins. The set of prescribed optical properties was compared to refractive indices of Saharan dust derived during the SAMUM-1 field campaign using different methods (Heinold et al., 2009). The assumed imaginary refractive indices represent the lower end of the range of the measurements, which reflects the remaining uncertainty in radiative forcing by Saharan dust (Tegen et al., 2010).

To compute radiative effects of biomass-burning aerosol (PM2.5), a mass extinction coefficient of $10\,\text{m}^2\,\text{g}^{-1}$ (250–700 nm) is used for the computation of smoke optical thickness. The mass extinction coefficient includes a factor for hygroscopic growth during transport, which is assumed to be constant at 1.35 (Reid et al., 2005), as a continuously high humidity was observed within the smoke layer. The single scattering albedo of smoke particles is 0.52 at 250–700 nm and 0.45 at 700–1530 nm wavelengths (Table 1). The optical properties represent highly absorbing smoke particles typical for African savanna fires in the flaming combustion phase. Several observations of intense mixed grass and slash fires and of fires in the earliest stages also reveal very high mass absorption efficiency values and single scattering values on the order of 0.3–0.6 (Reid et al., 2005, and references therein). Therefore, the wavelength-dependent optical properties of smoke particles used in this study are valid for local plumes. However, the single scattering albedo of smoke particles increases significantly with time due aging processes during transport (Reid et al., 2005). Accordingly, the results presented here are a maximum estimate of dust and smoke radiation effect. The model sensitivity to optical properties, which are more representative for the well-aged biomass particles over Cape Verde, will be tested in future model studies using results from the SAMUM-2 field campaign.

In addition to aerosol optical properties, the surface albedo is an important controlling parameter for radiative forcing (Bierwirth et al., 2009). The surface albedo in the standard COSMO version is based on soil type, soil moisture and coverage of vegetation, snow or ice. Particularly, the soil composition is still uncertain for most of the desert areas. As the standard surface albedo was found to be generally too low over the Saharan region when compared to satellite retrievals and local airborne observations (Tegen et al., 2010), it is replaced by a surface albedo map from MODIS measurements (Moody et al., 2005).

Table 1. Mie-derived single scattering albedo[a] ω_0 and asymmetry parameter g of Saharan dust and biomass burning aerosol particles used for the different radiation bands of COSMO as a function of dust effective radius r_e

			Effective radius r_e (μm)					
		Dust	0.17	0.5	1.5	4.6	13.8	Smoke	0.2
No.	Spectral band (μm)		$\omega_0/g \rightarrow$						
1	0.245–0.7		0.960/0.656	0.901/0.699	0.793/0.817	0.685/0.891	0.606/0.929		0.521/0.596
2	0.7–1.53		0.992/0.406	0.995/0.697	0.981/0.673	0.952/0.782	0.883/0.834		0.447/0.587
3	1.53–4.642		0.824/0.105	0.952/0.549	0.970/0.689	0.921/0.743	0.849/0.830		0.274/0.575
4	4.642–8.333		0.006/0.010	0.087/0.093	0.317/0.543	0.471/0.873	0.483/0.955		0.070/0.691
5	8.333–9.009, 10.309–12.5		0.003/0.004	0.058/0.036	0.358/0.308	0.520/0.699	0.543/0.859		0.104/0.612
6	9.009–10.309		0.006/0.004	0.105/0.035	0.421/0.247	0.569/0.628	0.631/0.759		0.101/0.544
7	12.5–20.0		0.000/0.001	0.010/0.013	0.165/0.118	0.442/0.543	0.543/0.801		0.091/0.677
8	20.0–104.515		0.000/0.001	0.004/0.006	0.083/0.055	0.408/0.303	0.496/0.678		0.075/0.603

[a]The values are spectrally integrated over the wavelength range of the corresponding spectral band.

To assess the radiative effects of dust and smoke particles, the episode is simulated twice: with radiatively active aerosol particles (model run: RAD) and without aerosol feedback on the COSMO radiation scheme (model run: CTL). The dust and smoke radiative forcing and the dynamic response are computed as differences between the results of both simulations. In reality, dust and biomass burning particles can act as cloud condensation nuclei and may contribute to the indirect aerosol effect. Here, the aerosol–cloud interactions are not considered, and there may be only a semi-direct effect on clouds. A cloud screening is applied to the model results to isolate the direct aerosol radiative impact from semi-direct effects and stochastic changes in cloud cover. For the analysis of the diagnosed radiative fluxes, grid cells with total cloud cover $\geq 1\%$ are excluded.

2.3. Measurements

This study makes use of the lidar observations at the airport of Praia/Santiago Island during the SAMUM-2 field campaign. Vertical profiles of the particle backscatter coefficient at 532 nm were measured with the Backscatter Extinction lidar-Ratio Temperature Humidity profiling Apparatus (BERTHA; Althausen et al., 2000; Tesche et al., 2009). The measurements together with the model results serve to illustrate the vertical distribution of dust and smoke layers over Praia. Following the method by Tesche et al. (2009), the backscatter coefficients are presented separately for dust and smoke particles.

During the campaign, nine flights were conducted with the research airplane Falcon from the German Aerospace Center (DLR). These flights were carried out over the Atlantic Ocean at different altitudes (below, in and above aerosol layers). The Modular Airborne Spectral Radiation Measurement System (SMART) Albedometer (Wendisch et al., 2001) was operated with an optical inlet to detect upward irradiance in the wavelength range 300–2200 nm (Bauer et al., 2011). Furthermore, lidar measurements (Esselborn et al., 2009) recorded vertical profiles of extinction coefficients below the aircraft, which were integrated to the values of AOT along the flight path. The airborne radiative measurements are compared to the modelled upward solar irradiances in the wavelength range 245–4642 nm for a case of Saharan dust with lofted biomass layer on 25 January 2008. The direct comparison will show whether the feedback simulations with COSMO-MUSCAT reveal reasonable estimates of radiative effects of dust and biomass-burning particles.

The space-borne lidar Cloud-Aerosol Lidar with Orthogonal Polarization (CALIOP) aboard Cloud-Aerosol Lidar and Infrared Pathfinder Satellite Observations (CALIPSO) provides information about the aerosol vertical distribution on a global scale. The CALIOP lidar emits two laser beams of linearly polarized light at 532 and 1064 nm and collects the laser light backscattered by molecules and particles at each level of altitude (Winker et al., 2007). At 532 nm wavelength, CALIOP horizontal resolution is 333 m below 8 km altitude and 1 km above. Profiles of the aerosol backscatter coefficient from the CALIPSO Lidar Level 2 data (ver. 2.01) at 40 km horizontal resolution and 532 nm wavelength are used to test the modelled aerosol layering computed with and without radiative feedback. The lidar profiles, which are contaminated by clouds are excluded from the analysis using the CALIPSO Lidar Level 2 Vertical Feature Mask (VFM). For model evaluation, the daily zonal mean of aerosol backscatter coefficient is computed from all transects of CALIPSO observations that cross the model domain during the course of a day.

3. Results

3.1. The plume of Saharan dust and biomass-burning particles

The radiative effects are investigated for the period from 25 January to 7 February 2008. The meteorological conditions were characterized by a strong south–north pressure gradient over the Sahel and southern Sahara caused by the intensity and southward extension of the Azores High (Knippertz et al., 2011). Accordingly, strong Harmattan winds and partly intense dust emissions and transport occurred in a latitudinal band from the Mauritanian coast to the Bodélé depression. Agricultural burning in the West African savannas was the main source of biomass burning aerosol observed over the Cape Verde Islands. The vegetation-fires were situated in an extended area between latitudes 5°N and 11°N from where the smoke plume was transported across the tropical Atlantic Ocean.

The spatial and temporal evolution of the mixed plume of Saharan dust and biomass burning aerosol is simulated with COSMO-MUSCAT. The model results have been comprehensively evaluated using routine ground-based and space-borne remote sensing and local field measurements in Heinold et al. (2011). They provide a detailed description of the dust and smoke events during the period of the SAMUM-2 field campaign. Thus, here only a brief overview is given. Figure 2 illustrates the modelled distribution of the mixed plume for the days 25 and 31 January 2008. Shown are maps of model-derived aerosol optical thickness (AOT) of dust/smoke (Figs 2a and b) and smoke particles (Figs 2c and d) at 550 nm. Blue areas in the maps indicate cloudy regions that are not considered for estimates of radiative effects. The mineral dust is advected from various sources of the western Sahara desert to Cape Verde by the Harmattan winds. Synoptic-scale midlevel easterlies prevail to the south and cause an efficient transport of biomass-burning aerosol from vegetation fires over southern West Africa (Fig. 2).

For the modelled period, a mean AOT of about 0.2 is computed for the Saharan desert (DES: 15°N–28°N; 13°W–25°E), 0.3 for the Sahel/Guinea Coast (SAH/GUI: 5°N–15°N; 10°W–20°E) and 0.6 for the tropical Atlantic Ocean (ATL: 2°N–25°N; 18°W–30°W) (see Fig. 1 for the location). Locally, AOT values of more than 4.4 are simulated during these days.

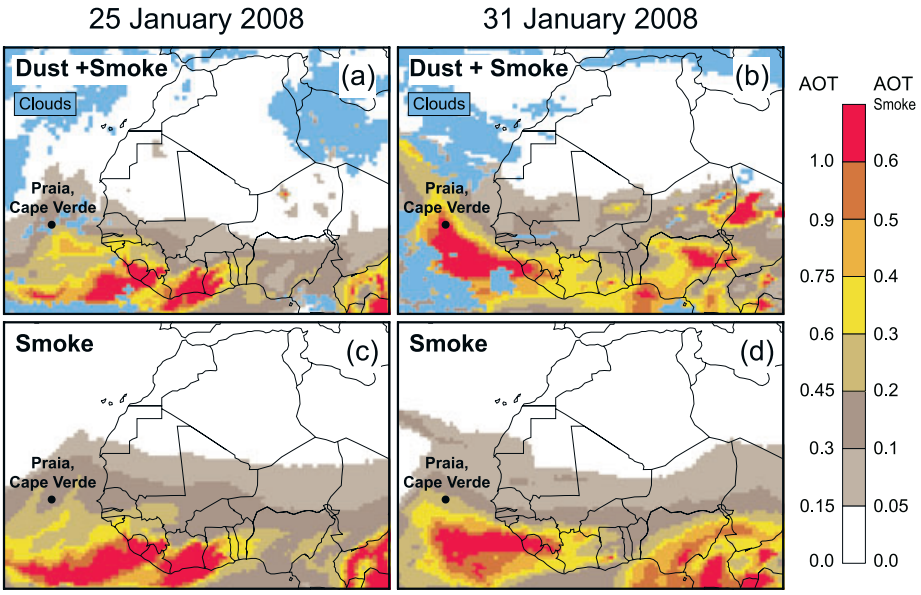

Fig. 2. Horizontal distribution of Saharan dust and biomass burning aerosol on 25 and 31 January 2008. Shown are maps of model-derived aerosol optical thickness (550 nm) of (a, b) the dust/smoke plume and (c, d) only smoke PM2.5. Note that the colour bar describes different units (modified from Heinold et al., 2011).

During the studied time period, mineral dust dominated the lowest 1.5 km of the atmosphere during intense dust events, but was also frequently mixed with the smoke plume. Layers of smoke were mainly present between 1 and 5 km height (Knippertz et al., 2011). This is shown by vertical profiles of backscatter coefficients taken during SAMUM-2 at Praia site and model results in Fig. 3. The backscatter coefficients are shown separately for dust and smoke aerosol. On 25 January

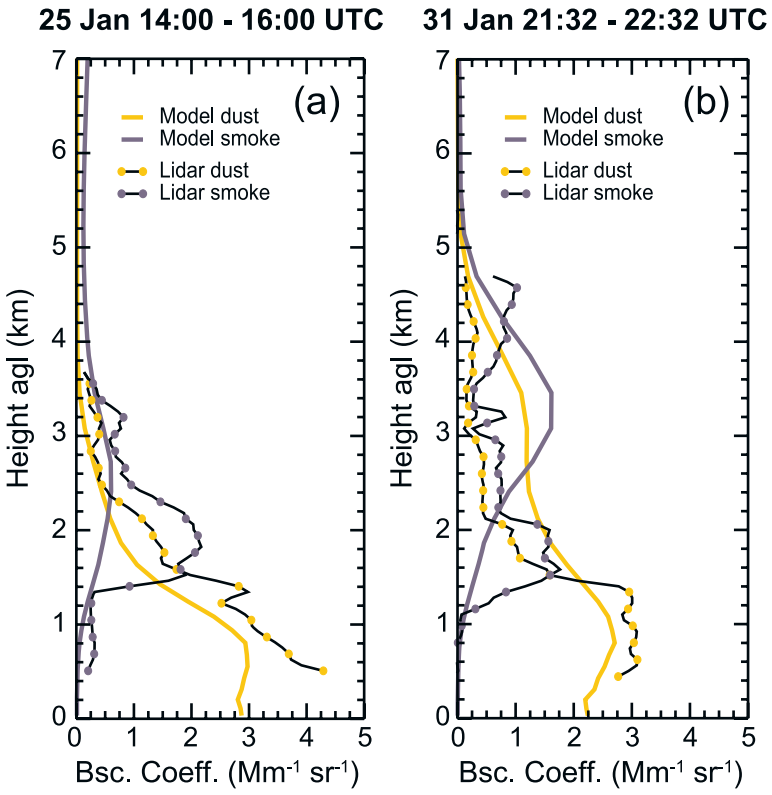

Fig. 3. Vertical profiles of dust (orange) and smoke (blue) particle backscatter coefficient (532 nm) at Praia site on 25 and 31 January 2008. Shown are modelled profiles (solid coloured lines) in comparison to lidar data (black lines with coloured circles) (modified from Heinold et al., 2011).

dust backscatter coefficients of up to 4–5 Mm^{-1} sr^{-1} were measured in the lowest 1 km above ground level (agl) over Praia. A layer of biomass-burning aerosol was centred at about 2 km height with a maximum backscatter coefficient of 4 Mm^{-1} sr^{-1}. The model mainly captures the actual layering of the mixed aerosol plume, although the backscatter coefficients of Saharan dust and biomass burning particles are underestimated in the simulations (Fig. 3a). Lidar measurements on 31 January indicate a well-mixed dust layer up to 1.4 km height. The dust-related backscatter coefficient reached values of about 3 Mm^{-1} sr^{-1}. A smoke plume extended from 1.2 to 4.8 km height. The maximum backscatter coefficients due to smoke particles ranged from 1 to 1.75 Mm^{-1} sr^{-1}. The magnitude of the model-derived dust backscatter coefficients agrees well with the observations, but the dust is too efficiently mixed to heights of about 5 km agl. In the model results, a more pronounced maximum of biomass burning aerosol is found at 3.5 km height (Fig. 3b).

3.2. *Radiative forcing of dust and smoke particles*

3.2.1. Comparison of modelled and measured radiative properties. Modelled upward solar irradiances are compared to radiation measurements from Falcon flights over the Atlantic Ocean on 25 January 2008 (Fig. 4). Saharan dust dominated the lowest 1.5 km of the atmosphere. Smoke layers were mainly present between 1 and 5 km height over the Cape Verde region (Fig. 3a). Values of measured AOT (only available from 15:09 UTC) range from 0.4 to 0.6. The modelled AOT remains at about 0.4 throughout the flight and agrees reasonably well with the observations. The measured upward solar irradiances slowly increase from 114 W m^{-2} during the departure phase as long as the flight level is situated within the aerosol layer. They reach values around 150 W m^{-2} with individual peaks up to 305 W m^{-2} due to underlying clouds. The modelled upward solar irradiances are 40% lower than the radiation measurements during the first 4 min when the aircraft flew below 5 km altitude. This is because, in contrast to the observations, clouds are simulated at higher levels dimming the incident and reflected solar radiation (see Fig. 2a for modelled cloud cover). The model results including aerosol–radiation interaction (RAD) are on average 10 W m^{-2} higher than the values from the control run without radiative feedback (CTL). Here, an increase in the effective albedo over the Atlantic ocean due to the presence of dust and smoke aerosol particles leads to an enhanced amount of upward solar radiation. For the remaining period, the non-feedback results are in agreement with the observations. However, the upward solar irradiances of the feedback run are on average 23% lower. The differences are caused by aerosol radiative effects under cloudy conditions. In the case with radiative feedback, dust and biomass-burning particles reduce the bright albedo of clouds, which are modelled below the aerosol layer (Fig. 4).

3.2.2. Estimates of direct net radiative forcing. The comparison of modelled and observed upward solar irradiances demonstrate that the coupled dynamic and radiation simulations give reasonable results for the following studies on radiative effects of dust and biomass burning smoke particles, even though the aerosol distribution is not always correctly reproduced.

In general, a better agreement between the modelled and observed aerosol distribution is found for the 31 January than for the 25 January (Heinold et al., 2011). Thus, in the following, the direct radiative effects of mineral dust and biomass burning aerosol particles are presented for the 31 January. They are quantified in terms of the radiative forcing for net (solar and terrestrial) radiation. It is defined as difference between the net

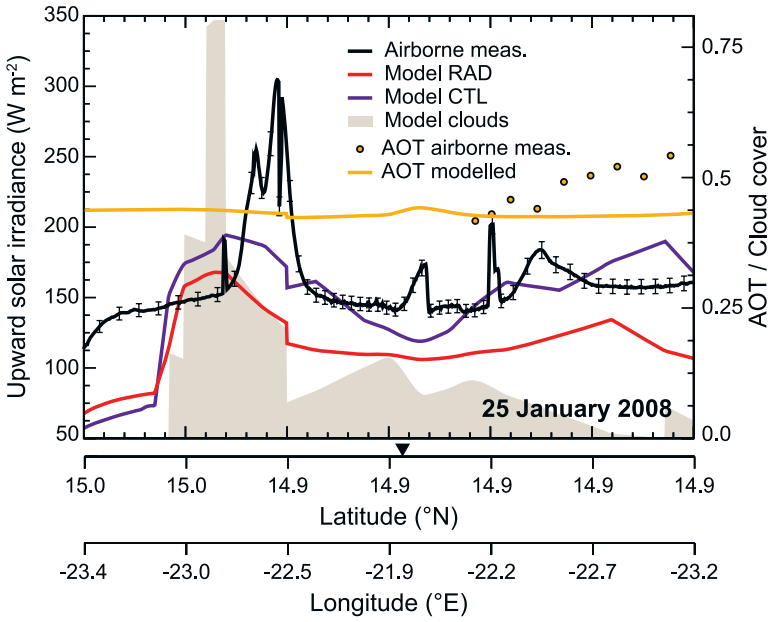

Fig. 4. Modelled aerosol optical thickness and upward solar irradiance compared with measurements taken during the Falcon flight west of Santiago Island on 25 January 2008 (14:50–15:20 UTC). The airborne radiation measurements were conducted under clear-sky conditions. The grey-shaded area indicates cloud coverage below the flight level in the model. The arrow on the latitude/longitude axis denotes the change in flight direction of the aircraft.

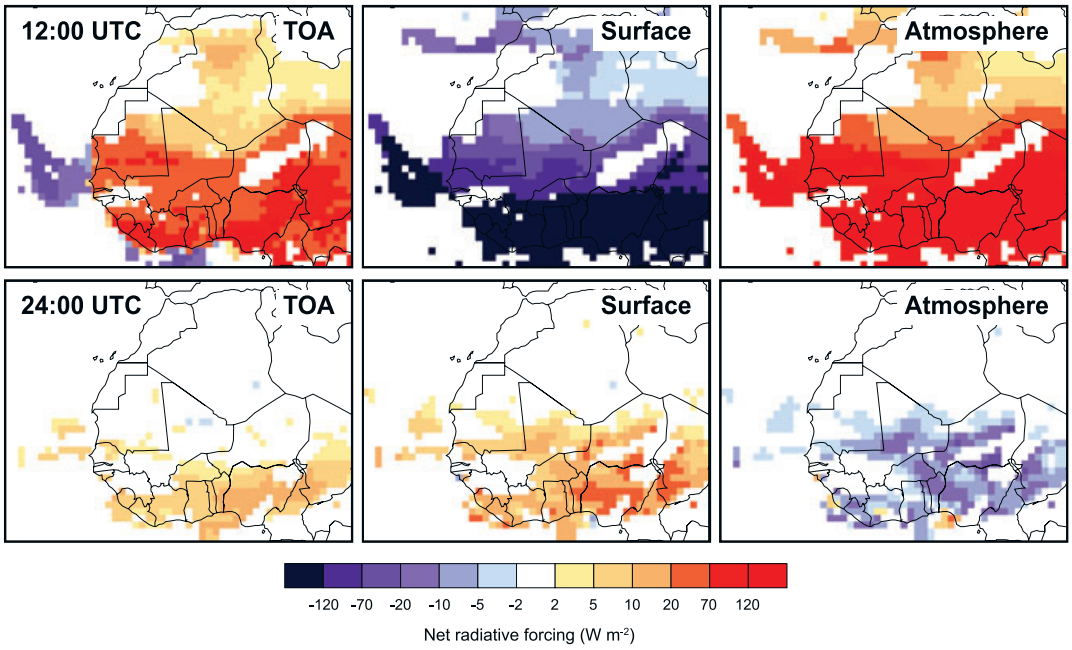

Fig. 5. Instantaneous net (solar and terrestrial) radiative forcing of modelled dust and smoke on 31 January 2008. Top: 12:00 UTC, lower: 24:00 UTC. Left: TOA forcing, centre: surface and right panels: atmospheric forcing (TOA minus surface forcing).

irradiance for the case without aerosol (subscript 'RAD') and with aerosol (subscript 'CTL') in the atmospheric column:

$$\Delta F = \left(F_{\downarrow} - F_{\uparrow}\right)_{\mathrm{RAD}} - \left(F_{\downarrow} - F_{\uparrow}\right)_{\mathrm{CTL}}, \qquad (2)$$

where $F_{\downarrow}$ and $F_{\uparrow}$ are the downward and upward directed irradiances, respectively. The clear-sky net radiative forcing computed for the 31 January 2008 is shown as an example in Fig. 5. Its sign is determined by the surface albedo and the optical properties of aerosol particles. During noontime, the albedo over the sea is increased by the dust and biomass-burning smoke layer leading to an enhanced flux of upward solar radiation. Therefore, there is a negative instantaneous radiative forcing over the Atlantic Ocean, which reaches up to -47 W m^{-2}. Over the Sahara and southern West Africa, dust and smoke particles cause a reduction of surface albedo and an instantaneous net radiative forcing at top of the atmosphere (TOA) at 12:00 UTC that is always positive with locally up to $+152$ W m^{-2}. The mixture of dust and smoke decreases the atmospheric transmission, which reduces the incoming solar radiation at the surface. The instantaneous net radiative forcing at surface is generally negative reaching a maximum of -627 W m^{-2}. Because of absorption of incident solar radiation within the overlying aerosol layer, the net atmospheric forcing (TOA minus surface forcing) is always positive with locally up to $+721$ W m^{-2}. At night, the dominant aerosol radiative effect is the reduction of the outgoing terrestrial radiation in comparison to a atmosphere without dust and smoke. The absence of the solar effect leads to a positive instantaneous net radiative forcing of up to $+43$ W m^{-2} at surface and $+16$ W m^{-2} at TOA. The net atmospheric forcing of mineral dust and biomass burning smoke particles is mainly negative with locally up to -34 W m^{-2}.

Table 2. Averaged instantaneous net radiative forcing and forcing efficiency of the mixed dust and smoke plume for the surface, TOA and the atmospheric column. The values represent averages over the period 25 January–7 February and the regions: Saharan desert (15°N–28°N; 13°W–25°E), Sahel/Guinea Coast (5°N–15°N; 10°W–20°E) and tropical Atlantic Ocean (2°N–25°N; 18°W–30°W).

	Surface	TOA	Atmosphere
Radiative forcing (W m^{-2})			
Sahara desert	−14	+16	+30
Sahel region	−39	+19	+58
Atlantic Ocean	−19	±0	+19
Radiative forcing efficiency (W m^{-2})			
Sahara desert	−67	+77	+143
Sahel region	−93	+53	+145
Atlantic Ocean	−42	±0	+42

Mean radiative effects of mineral dust and biomass burning smoke particles are summarized in Table 2 in terms of daily averaged instantaneous net radiative forcing and radiative forcing efficiencies. The values are given for the surface, TOA and the atmosphere averaged over the period 25 January to 7 February and the regions: Saharan desert (DES: 15°N–28°N; 13°W–25°E), Sahel/Guinea Coast (SAH/GUI: 5°N–15°N; 10°W–20°E) and tropical Atlantic Ocean (ATL: 2°N–25°N; 18°W–30°W). The mean instantaneous net forcing at surface is also negative and

ranges from -14 to -39 W m^{-2} for the Saharan desert and the Sahel/Guinea region. At TOA, the values are positive with up to $+19$ W m^{-2} over land. However, negative and positive radiative forcings at day- and nighttime, respectively, cancel each other out on daily average over the Atlantic Ocean. The absorption of incident solar radiation by dust and smoke particles leading to a positive net atmospheric forcing during daytime hours predominate over the negative effect due to the reduction of the outgoing terrestrial radiation at night. As a consequence, the mean net atmospheric forcing is always positive reaching $+58$ W m^{-2}.

To exclude the impact of the aerosol particle concentration, the forcing efficiency $\Delta F/\tau$, which is the radiative forcing produced by a unit of AOT, is given as daily mean for the three regions and for AOT values exceeding 0.1 at 550 nm wavelength (Table 2). As for the values of radiative forcing, the forcing efficiencies are dominated by the daytime effect. Dust and smoke particles cause a reduction of surface albedo over the Sahara and the Sahel/Guinea region. The TOA radiative effect of dust over the bright Saharan surface ($+77$ W m^{-2}) is 45% greater than the effect of dust and smoke layers covering the Sahel and Guinea Coast regions ($+53$ W m^{-2}) with lower albedo. However, the forcing efficiency for the atmosphere is nearly the same with about $+145$ W m^{-2} on average over both regions. This indicates that, as expected, the mixture of mineral dust and biomass burning particles absorbs more effectively than pure dust. Thus, the mean forcing efficiency at surface is more negative with -93 W m^{-2} over southern West Africa than over the Sahara (-67 W m^{-2}). For the Atlantic ocean, the amount of the radiative forcing efficiency is 42 W m^{-2} at surface (negative) and for the atmosphere (positive).

3.3. *Feedback on atmospheric dynamics and aerosol transport*

The atmospheric response to dust and smoke radiative effects is presented in terms of temperature and air pressure changes in Fig. 6. Shown are differences of the 500 and 950 hPa temperature and the surface pressure computed from model results of radiative feedback and non-feedback runs. The maps show difference values for 12:00 and 24:00 UTC and for the daily mean each averaged over the period 25 January to 7 February.

There is a yield of radiative energy in the atmospheric column, which is caused by the absorption of solar and terrestrial radiation within the plume of mineral dust and biomass burning smoke. This effect is evident throughout the day in the overall increase in the 500 hPa temperature reaching up to $+1.1$ K over the southern West African coast (Fig. 6, upper). The differences in the horizontal distribution of atmospheric response during different times of the day are mainly related to the spatial and temporal evolution of the aerosol plume.

The negative surface forcing results in a decrease in the near-surface (950 hPa) temperature over land (Fig. 6, centre). Strongest reductions of locally up to 2.7 K on average occur in regions with highest AOT at noontime. Although terrestrial radiative energy is partly trapped between surface and aerosol layer preventing the surface from cooling, the simulated planetary boundary layer (PBL) temperature at night is still lower when including radiative feedback because of the strong radiative cooling during daytime. The sea surface temperature is fixed at an initial state and does not respond to the dust and smoke radiative forcing. Nevertheless, negative temperature effects are computed at the 950 hPa level west of the African continent and positive ones off the Guinea cost. This is due to the fact, that the cooled dust-laden PBL air masses are advected off the West African coast. Whereas to the south, the near-surface smoke dominated aerosol heats the lowest atmospheric layers due to absorption of solar radiation and preventing outgoing terrestrial radiation being lost to space while the sea surface heat flux remains constant. The positive temperature effect is reinforced at night reaching 1.6 K off the coast of Guinea Bissau as the radiative effects are established at the end of a 48-h model cycle. Therefore, the main daytime effect of the mixed dust and biomass-burning smoke plume is to redistribute radiative heating from the surface to the atmospheric column over land, as has been already shown in earlier studies for pure mineral dust (e.g. Miller et al., 2004; Tulet et al., 2008) and biomass-burning particles (e.g. Ramanathan et al., 2001; Johnson et al., 2008).

As shown in Fig. 6 (lower), the radiative impact of dust and smoke particles on temperature fields corresponds to variations of the air pressure. The aerosol radiative heating within the aerosol plume extends over several vertical layers and induces rising motion and negative pressure perturbations near the surface. The overall decrease of surface pressure ranges from about 5 to 118 Pa at daytime and 82 Pa on daily average. Owing to a pronounced radiative cooling near the aerosol layer top (not shown) and at surface, the simulations reveal sinking motion and pressure increase over the biomass burning area at night. For the remaining domain, the negative radiative effect on surface pressure prevails.

Differential heating/cooling and associated pressure disturbances due to the radiative forcing by mineral dust and biomass burning aerosol particles feed back on atmospheric dynamics. The air-flow patterns are locally modified as indicated by white arrows in Fig. 6 (lower). The response to the aerosol forcing results in both increase and decrease of surface wind speeds. Regions of convergence form at surface off the Guinea coast and over western Central Africa, where highest dust and smoke concentrations are modelled. In addition, the Hadley circulation is enhanced when dust and smoke radiative forcing is considered in the simulations. As a quantitative measure of the strengthening of the Hadley cell, mean pressure gradients are computed from modelled pressure fields between $5 \pm 2.5^{\circ}$N and $30 \pm 2.5^{\circ}$N over the Atlantic Ocean (30°W–18°W) from 25 January to 7 February. At surface, the south–north gradient of surface

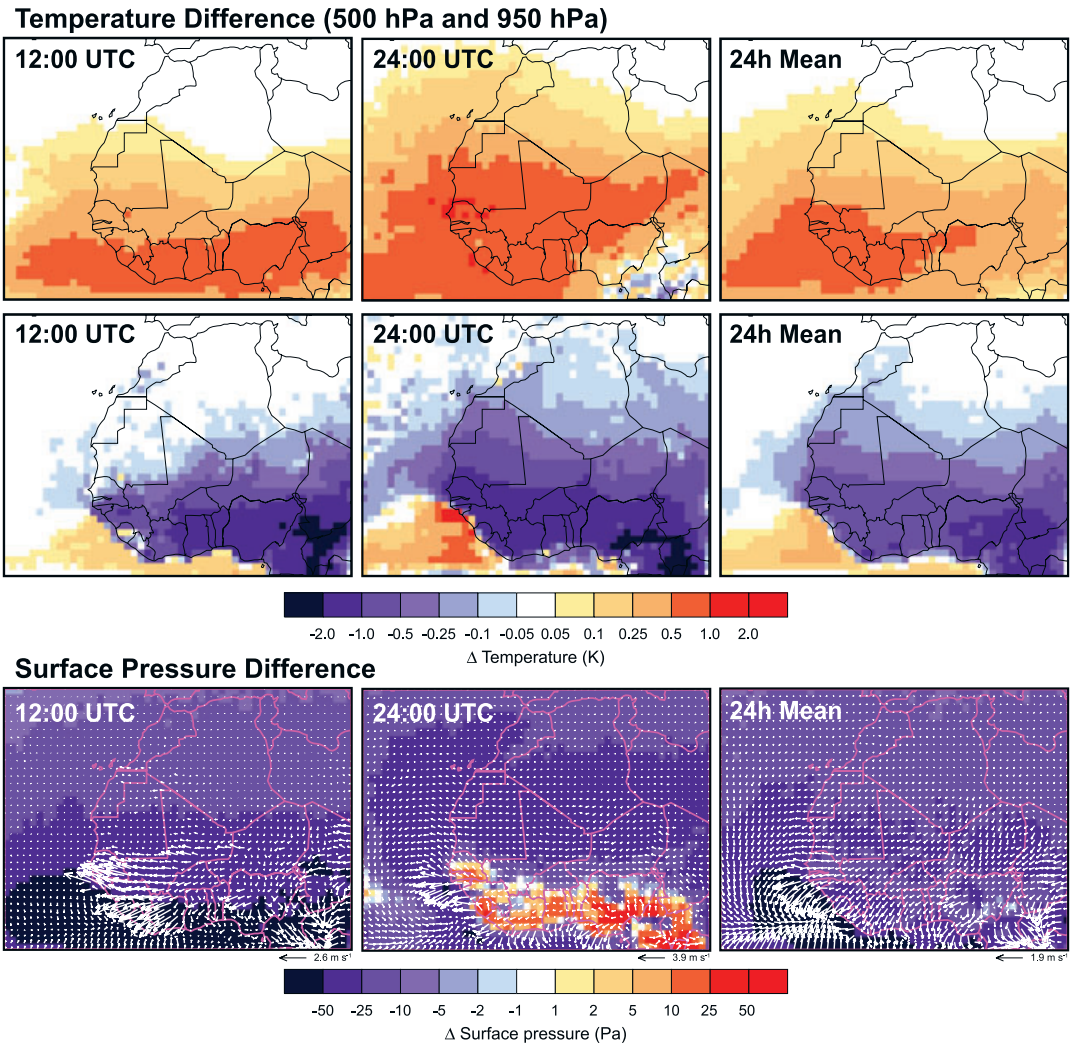

Fig. 6. Difference maps of the modelled temperature between the experiment including aerosol radiative forcing (RAD) and results when the feedback is not included (CTL), averaged over the period from 25 January to 7 February 2008. Top: 500 hPa level, centre panels: 950 hPa level. Left: 12:00 UTC, centre: 24:00 UTC and right panels: daily mean. Lower: corresponding mean difference in modelled surface pressure. Note the use of a logarithmic colour scale. White arrows denote changes in surface winds induced by dust and smoke radiative forcing (zonal and meridional wind speed differences between case RAD and CTL).

pressure is increased by 30 Pa, whereas at the 500 hPa level the north–south pressure gradient is also increased by 12 Pa. The values indicate a systematically enhanced Hadley circulation, which leads to stronger upper-level air transport. In accordance, Wang (2007) and Lau et al. (2009) found similar effects on the Northern Hemisphere Hadley cell due to biomass-burning particles and Saharan dust, respectively. The findings demonstrate that the influence of dust and smoke radiative forcing does not only affect the boundary layer meteorology but also the synoptic-scale circulation.

The impact of the radiative effects and feedbacks on the aerosol transport itself is discussed by means of maps of AOT and their differences. The changes in the horizontal distribution of mineral dust and biomass-burning smoke are shown exemplary for 31 January 2008 at 12:00 UTC (Fig. 7). As a result of the enhanced Hadley circulation, smoke particles are advected further north by more than 5° in the radiative feedback simulations. In contrast, the equatorward transport is reduced, and biomass-burning material concentrates in the convergence zones along the Guinea coast and over Nigeria (Fig. 7, left).

Aerosol–radiation interactions can affect the emission of mineral dust (Ahn et al., 2007; Heinold et al., 2008). However, these effects can be neglected compared with the perturbation of transport processes. In this case, the direct radiative forcing caused an increase in total Saharan dust emissions of only 3%. Flow patterns in Fig. 6 (lower) show a cyclonic circulation west of the African continent induced by the dust and smoke radiative forcing. Therefore, the transport of Saharan dust is more focused

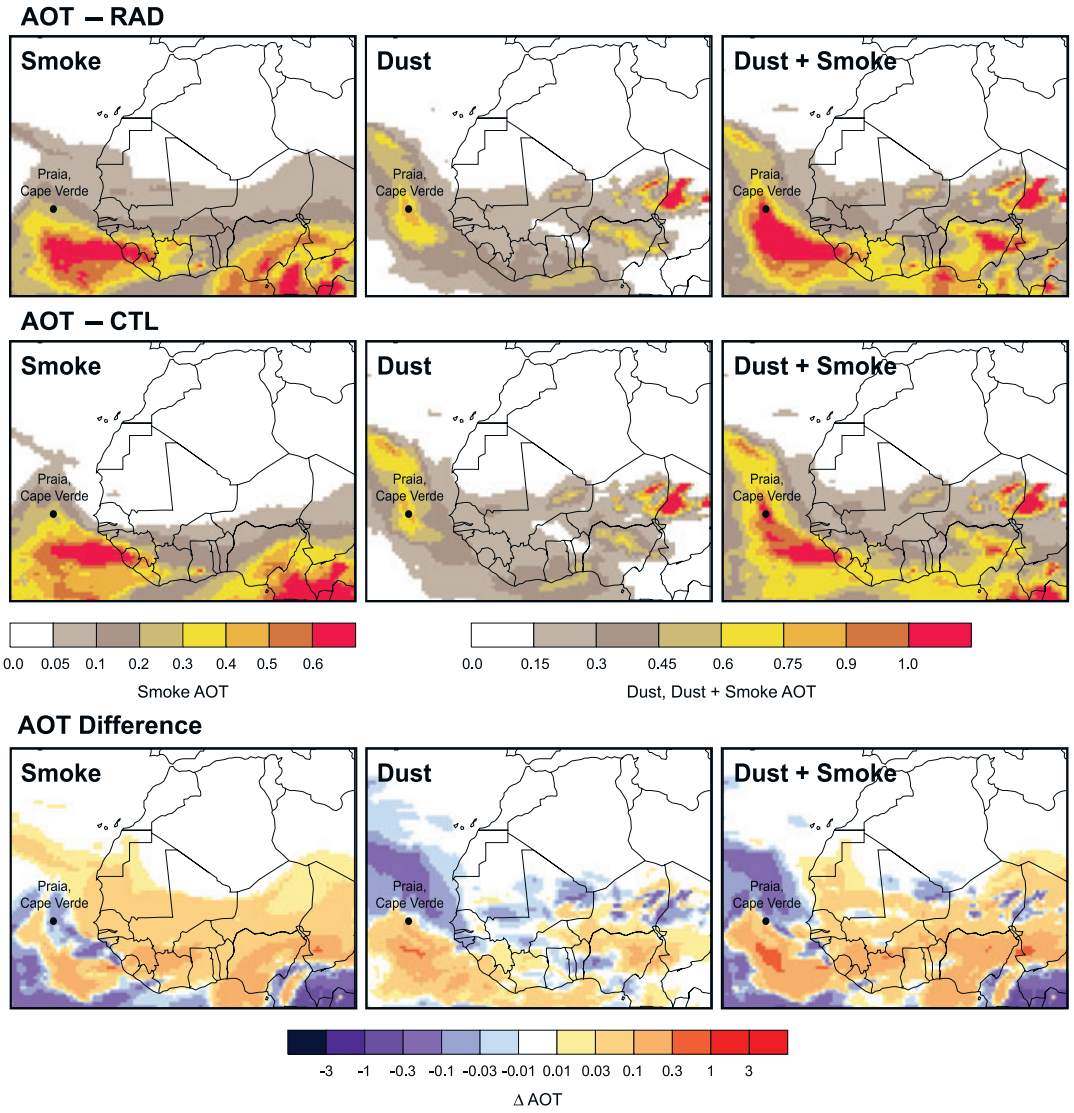

Fig. 7. Maps of model-derived aerosol optical thickness on 31 January 2008, 12:00 UTC. Top panels: radiative feedback simulation. Lower: control run. Left panels: biomass burning aerosol, centre: Saharan dust and right panels: total of smoke and dust. Note the use of different colour bars for smoke and dust/total aerosol.

towards the Cape Verde region compared to the model results without radiative feedback (Fig. 7, centre).

Combining the effects on dust and biomass-burning smoke advection, the total AOT values are partly increased by more than 40% over the tropical Atlantic Ocean and the Bight of Benin, whereas there is a reduction in AOT in western Central Africa and across the Atlantic Ocean north of 20°N.

Figures 8(a)–(c) show the daily zonal mean of aerosol backscatter coefficient computed from all meridian transects of CALIPSO observations and corresponding model results crossing the model domain on 31 January 2008. The layer of Saharan dust and biomass burning aerosol is reasonably reproduced considering the difficulties in comparing model results to space-borne lidar measurements. The model underestimates the maximum backscatter coefficients by a factor of at least 2, and dust layers north of about 21°N are not simulated. It cannot be decided whether the model results with or without radiative feedback agree better with the CALIPSO profiles. Still, differences are evident in the meridian cross-sections. In particular, the aerosol layer top is more vertically structured when aerosol radiative feedback is considered, which is closer to reality (Figs 8a–c). Locally, the vertical distribution of the modelled biomass burning plume is improved with radiatively active aerosol particles as comparisons with lidar observations at the SAMUM-2 field site Praia show. The lidar profile on 31 January (Fig. 8d) indicates the presence of smoke particles between 1 and 5 km with maximum extinction coefficients of about 105 and 75 Mm^{-1} at 1.8 and 4.2 km height, respectively. In the model run without

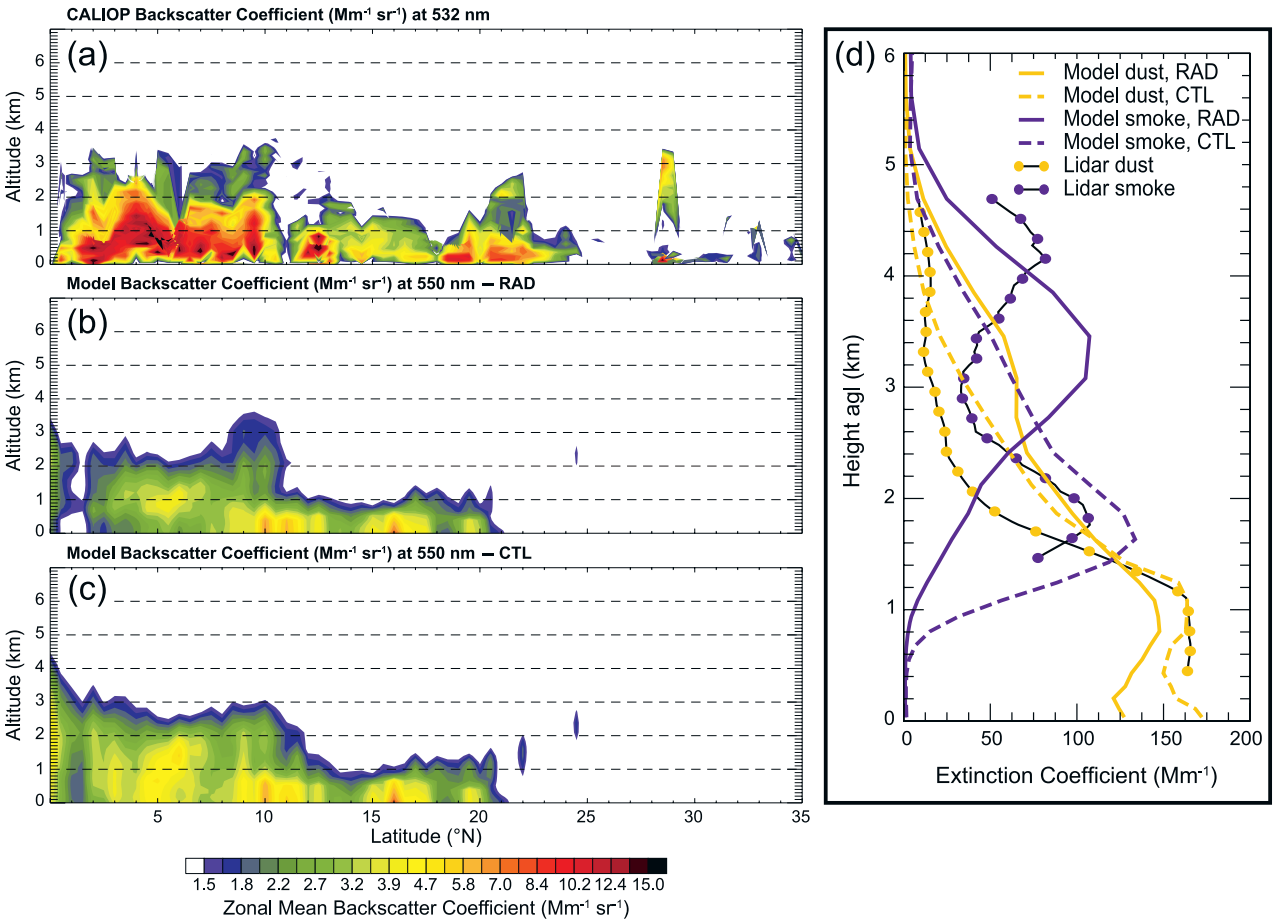

Fig. 8. Daily-mean vertical layering of dust and biomass burning smoke on 31 January 2008 averaged over the model domain. Shown are transects of backscatter coefficients (a) measured onboard CALIPSO satellite and computed using COSMO-MUSCAT (b) with and (c) without radiative feedback. (d) Vertical profiles of dust (orange) and smoke (blue) backscatter coefficients (532 nm) at Praia site on 31 January (21:32–22:32 UTC) 2008. Comparison of modelled profiles from feedback simulation (solid coloured lines) and from control run (dashed coloured lines) with lidar data (black lines with coloured circles).

radiative feedback, the vertical transport of smoke is underestimated. Although the location of the lowest smoke layer is reproduced, the values of the extinction coefficient steadily decrease above this height. The two maximal of the smoke extinction coefficient are also not resolved in the feedback simulations, but a single layer of biomass-burning aerosol centred in about 3.5 km is computed within the correct height range. As mention above, the transport of mineral dust is more directed towards the Cape Verde Islands when the radiative feedback is included. However, this increases the tendency to overestimate the dust load above 1.5 km height caused by a too strong vertical mixing in the model (Heinold et al., 2011).

4. Summary and conclusions

The radiative forcing and feedbacks on atmospheric dynamics by Saharan dust and biomass-burning aerosol particles were investigated for a case study during the SAMUM-2 field experiment in the Cape Verdes in January and February 2008. The spatial and temporal evolution of the dust and smoke plume was simulated using the regional model system COSMO-MUSCAT. The coupled dynamic–radiation model allows online interaction of the modelled dust and smoke particle concentration with the solar and terrestrial radiation and with the model dynamics. The optical properties of mineral dust were computed from the size-resolved dust load assuming a mineral composition containing 2% haematite, which is highly absorbing at solar wavelengths. The prescribed dust refractive indices were chosen in accordance with measurements in the vicinity of dust sources during the SAMUM-1 field campaign. High values of absorption were also assumed for biomass burning PM2.5 representative for freshly emitted smoke particles from African savanna fires during the flaming phase and intense mixed grass/slash fires. Thus, the findings on the smoke radiative feedback should be considered as the maximum effects that can be expected.

In a first step, the modelled upward solar irradiances were evaluated against airborne radiative measurements over the Atlantic Ocean for a case of biomass burning aerosol above desert dust. The comparison showed that the observations were well reproduced and that the feedback simulations provide a reasonable basis for estimating the radiative effects of dust and biomass-burning smoke particles.

The results presented here for the clear-sky net radiative forcing of the mixture of mineral dust and biomass smoke are negative on daily average reaching $-39\ \mathrm{W\,m^{-2}}$ for the 14-day period. At TOA and for the atmosphere, the values are positive with up to $+19$ and $+58\ \mathrm{W\,m^{-2}}$, respectively. The impact of the presence of dust and smoke particles on atmospheric dynamic is due to changes in the atmospheric radiative heating rates. At daytime, atmospheric layers comprising the aerosol plume are heated by absorption whereas the surface is cooled as incident radiation is reduced. This results in an overall decrease of the surface pressure between 5 and 118 Pa at daytime and 82 Pa for the diurnal mean averaged over 14 days. The differential atmospheric heating/cooling and related pressure perturbations modify the air-flow patterns at local and synoptic scale. The Hadley circulation is enhanced and convergence zones form along the Guinea coast. As a consequence, smoke particles are transported further north by more than 5° in the radiative feedback simulations whereas the equatorward aerosol transport is reduced. Within the areas of convergence induced by radiative feedback, Saharan dust and biomass-burning material are more directed towards the Cape Verde region and the Bight of Benin.

The model results indicate that including the radiative forcing in dust and biomass-burning simulations makes a difference to atmospheric dynamics, which should be considered. The impact of Saharan dust and smoke particles on the radiation budget is part of the complex West African circulation. It influences the meteorological conditions at different scales, but also affects the aerosol transport itself broadening its relevance to air quality and climate issues. However, it could not be shown if model runs with aerosol–radiation interaction generally agree better with aerosol observations than those without radiative feedback given the uncertainties in the model. An improvement of the vertical smoke distribution was found locally. Measurements are principally insufficient to directly validate the dynamic feedbacks, as in nature, only the combined effects of radiative processes and atmospheric coupling can be observed.

In this context, the fixed sea-surface temperature in the model was problematic, since the constant surface heat flux together with the terrestrial aerosol forcing led to an unrealistic heating of the marine boundary layer. Thus, future model versions should allow the sea surface temperature to respond to aerosol radiative effects, which is already common in global scale, but not in regional scale models.

A major goal of the SAMUM-2 project was to clarify the uncertainties in radiative properties of the mixed plume of Saharan dust and biomass burning smoke particles by different independent measurements. The investigation of the smoke particle properties during the field campaign result in a range of 0.6–0.9 (Tesche et al., 2011; Müller et al., 2011) for the single scattering albedo at 530 nm wavelength. Biomass burning optical properties are controlled by manifold factors such as the vegetation type burned, the relative contribution of the flaming and smouldering combustion phases and the state of particle aging (Dubovik et al., 2002; Reid et al., 2005). The optical properties used in this study are typical for local smoke plumes with high values of absorption. In a follow-up study, the sensitivity of radiative effects and feedbacks to smoke optical properties will be investigated including tests of smoke optical parameters which better represent the well-aged smoke particles observed over Cape Verde.

In addition, a closer look is required at the role of sea salt, which was often observed below 1 km during the campaign (Knippertz et al., 2011), but was not yet considered in the simulations. Sea salt characterized by low values of mass absorption and high single scattering albedos (Müller et al., 2011) can impact the radiative forcing by dust and smoke aerosol particles. It is expected to enhance the positive solar TOA radiative forcing of a lofted dust and biomass layer depending on surface albedo and aerosol optical properties.

5. Acknowledgments

The SAMUM (Saharan Mineral Dust Experiment) researcher group is funded by the German Science Foundation (DFG) under Grant FOR539. The CALIPSO data were obtained from the NASA Langley Research Center Atmospheric Sciences Data Center. We also acknowledge good cooperation and support from the German weather service 'Deutscher Wetterdienst' (DWD) and the John von Neumann Institute for Computing (Jülich). The MODIS land product data are distributed by the Land Processes Distributed Active Archive Center (LP DAAC), located at the U.S. Geological Survey (USGS) Earth Resources Observation and Science (EROS) Center (lpdaac.usgs.gov).

References

Ahn, H. J., Park, S. U. and Chang, L. S. 2007. Effect of direct radiative forcing of Asian dust on the meteorological fields in east Asia during an Asian dust event period. *J. Appl. Meteorol. Climatol.* **46**, 1655–1681.

Althausen, D., Müller, D., Ansmann, A., Wandinger, U., Hube, H. and co-authors. 2000. Scanning 6-wavelength 11-channel aerosol lidar. *J. Atmos. Oceanic Technol.* **17**, 1469–1482.

Andreae, M. O. and Merlet, P. 2001. Emission of trace gases and aerosols from biomass burning. *Global Biogeochem. Cycles* **15**, 955–966.

Ansmann, A., Petzold, A., Kandler, K., Tegen, I., Wendisch, M. and co-authors. 2011. Saharan Mineral Dust Experiments SAMUM–1 and SAMUM–2: What have we learned? *Tellus* **63B**, this issue.

Barbosa, P. M., Stroppiana, D., Gregoire, J. M. and Pereira, J. M. C. 1999. An assessment of vegetation fire in Africa (1981–1991): burned

areas, burned biomass, and atmospheric emissions. *Glob. Biogeochem. Cycle* **13**, 933–950.

Bauer, S., Bierwirth, E., Esselborn, M., Petzold, A., Macke, A. and co-authors. 2011. Airborne spectral radiation measurements to derive solar radiative forcing of Saharan dust mixed with biomass burning smoke particles. *Tellus* **63B**, this issue.

Bierwirth, E., Wendisch, M., Ehrlich, A., Heese, B., Tesche, M. and co-authors. 2009. Spectral surface albedo over Morocco and its impact on the radiative forcing of Saharan dust. *Tellus* **61B**, doi:10.1111/j.1600-0889.2008.00395.x.

Dubovik, O., Holben, B., Eck, T. F., Smirnov, A., Kaufman, Y. J. and co-authors. 2002. Variability of absorption and optical properties of key aerosol types observed in worldwide locations. *J. Atmos. Sci.* **59**, 590–608.

Esselborn, M., Wirth, M., Fix, A., Weinzierl, B., Rasp, K. and co-authors. 2009. Spatial distribution and optical properties of Saharan dust observed by airborne high spectral resolution lidar during SAMUM 2006. *Tellus* **61B**, doi:10.1111/j.1600-0889.2008.00394.x.

Haywood, J. and Boucher, O. 2000. Estimates of the direct and indirect radiative forcing due to tropospheric aerosols: a review. *Rev. Geophys.* **38**(4), 513–543.

Haywood, J. M., Pelon, J., Formenti, P., Bharmal, N., Brooks, M. and co-authors. 2008. Overview of the dust and biomass-burning experiment and African Monsoon multidisciplinary analysis special observing period-0. *J. Geophys. Res.* **113**, doi:10.1029/2008JD010077.

Heinold, B., Tegen, I., Schepanski, K. and Hellmuth, O. 2008. Dust radiative feedback on Saharan boundary layer dynamics and dust mobilization. *Geophys. Res. Lett.* **35**, L20817, doi:10.1029/2008GL035319.

Heinold, B., Tegen, I., Esselborn, M., Kandler, K., Knippertz, P. and co-authors. 2009. Regional Saharan dust modelling during the SAMUM 2006 campaign. *Tellus* **61B**, doi:10.1111/j.1600-0889.2008.00387.x.

Heinold, B., Tegen, I., Schepanski, K., Tesche, M., Esselborn, M. and co-authors. 2011. Regional modelling of Saharan dust and biomass burning smoke – Part 1: Model description and evaluation. *Tellus* **63B**, this issue.

Helmert, J., Heinold, B., Tegen, I., Hellmuth, O. and Wendisch, M. 2007. On the direct and semi-direct effect of Saharan dust over Europe: a modeling study. *J. Geophys. Res.* **112**, D11204, doi:10.1029/2006JD007444.

Johnson, B. T., Heese, B., McFarlane, S. A., Chazette, P., Jones, A. and co-authors. 2008. Vertical distribution and radiative effects of mineral dust and biomass burning aerosol over West Africa during DABEX. *J. Geophys. Res.* **113**(D17), D00C12, doi:10.1029/2008JD009848.

Kalu, A. E. 1979. The African dust plume: its characteristics and propagation across West Africa in winter. In: *Saharan Dust* (ed. C. Morales), J. Wiley and Sons, Chichester, 95–118

Kaufman, Y. J., Koren, I., Remer, L. A., Tanré, D., Ginoux, P. and co-authors. 2005. Dust transport and deposition observed from the Terra-Moderate Resolution Imaging Spectroradiometer (MODIS) spacecraft over the Atlantic ocean. *J. Geophys. Res.* **110**, doi:10.1029/2003JD004436.

Knippertz, P., Tesche, M., Heinold, B., Kandler, K., Schladitz, A. and co-authors. 2011. Dust mobilization and transport from West Africa to Cape Verde—a meteorological overview of SAMUM–2. *Tellus* **63B**, *this issue*.

Lau, K. M., Kim, K. M., Sud, Y. C. and Walker, G. K. 2009. A GCM study of the response of the atmospheric water cycle of West Africa and the Atlantic to Saharan dust radiative forcing. *Ann. Geophys.* **27**(10), 4023–4037.

Majewski, D., Liermann, D., Prohl, P., Ritter, B., Buchhold, M. and co-authors. 2002. The operational global icosahedral-hexagonal gridpoint model GME: Description and high-resolution tests. *Mon. Wea. Rev.* **130**(2), 319–338.

Malavelle, F., Pont, V., Mallet, M., Solmon, F., Johnson, B. and co-authors. 2011. Simulation of aerosol radiative effects over West Africa during DABEX and AMMA SOP-0. *J. Geophys. Res.* **116**, D08205, doi:10.1029/2010JD014829.

Miller, R. L., Perlwitz, J. and Tegen, I. 2004. Feedback upon dust emission by dust radiative forcing through the planetary boundary layer. *J. Geophys. Res.* **109**(D24), D24209, doi:10.1029/2004JD004912.

Moody, E. G., King, M. D., Platnick, S., Schaaf, C. B. and Gao, F. 2005. Spatially complete global spectral surface albedos: value-added datasets derived from terra MODIS land products. *IEEE Trans. Geosci. Remote Sensing* **43**, 144–158, doi:10.1109/TGRS.2004.838359.

Müller, T., Schladitz, A. and Wiedensohler, A. 2011. Spectral particle absorption coefficients, single scattering albedos, and imaginary parts of refractive indices at Cape Verde Island during SAMUM–2. *Tellus* **63B**, this issue.

Myhre, G., Grini, A., Haywood, J. M., Stordal, F., Chatenet, B. and co-authors. 2003. Modeling the radiative impact of mineral dust during the Saharan Dust Experiment (SHADE) campaign. *J. Geophys. Res.* **108**(D18), 8579, doi:10.1029/2002JD002566.

Myhre, G., Hoyle, C. R., Berglen, T. F., Johnson, B. T. and Haywood, J. M. 2008. Modeling of the solar radiative impact of biomass burning aerosols during the Dust and Biomass-burning Experiment (DABEX). *J. Geophys. Res.* **113**, D00C16, doi:10.1029/2008JD009857.

Pérez, C., Nickovic, S., Pejanovic, G., Baldasano, J. M. and Özsoy, E. 2006. Interactive dust-radiation modeling: a step to improve weather forecasts. *J. Geophys. Res.* **111**(D16), doi:10.1029/2005JD006.

Ramanathan, V., Crutzen, P. J., Kiehl, J. T. and Rosenfeld, D. 2001. Atmosphere – aerosols, climate, and the hydrological cycle. *Science* **294**, 2119–2124.

Reid, J. S., Eck, T. F., Christopher, S. A., Koppmann, R., Dubovik, O. and co-authors. 2005. A review of biomass burning emissions part III: intensive optical properties of biomass burning particles. *Atmos. Chem. Phys.* **5**, 827–849.

Renner, E. and Wolke, R. 2010. Modelling the formation and atmospheric transport of secondary inorganic aerosols with special attention to regions with high ammonia emissions. *Atmos. Environ.* **44**(15), 1904–1912, doi:10.1016/j.atmosenv.2010.02.018.

Ritter, B. and Geleyn, J. F. 1992. A comprehensive radiation scheme for numerical weather prediction models with potential applications in climate simulations. *Mon. Wea. Rev.* **120**, 303–325.

Schepanski, K., Tegen, I., Todd, M. C., Heinold, B., Bönisch, G. and co-authors. 2009, Meteorological processes forcing Saharan dust emission inferred from MSG-SEVIRI observations of subdaily dust source activation and numerical models. *J. Geophys. Res.* **114**, doi:10.1029/2008JD010325.

Sokolik, I. N. and Toon, O. B. 1996. Direct radiative forcing by anthropogenic airborne mineral aerosols. *Nature* **381**, 681–683.

Sokolik, I. N. and Toon, O. B. 1999. Incorporation of mineralogical composition into models of the radiative properties of mineral aerosol from UV to IR wavelengths. *J. Geophys. Res.* **104**, 9423–9444.

Solmon, F., Mallet, M., Elguindi, N., Giorgi, F., Zakey, I. and co-authors. 2008. Dust impact on sahelian precipitation gradients, mechanisms and sensitivity to absorption properties. *J. Geophys. Res.* **35**, L24705, doi:10.1029/2008GL035900.

Steppeler, J., Doms, G., Schättler, U., Bitzer, H. W., Gassmann, A. and co-authors. 2003. Meso-gamma scale forecasts using the nonhydrostatic model LM. *Meteorol. Atmos. Phys.* **107**(D21), 4576, doi:10.1007/s00703-001-0592-9, 75–96.

Tegen, I., Bierwirth, E., Heinold, B., Helmert, J. and Wendisch, M. 2010. Effect of measured surface albedo on modeled Saharan dust solar radiative forcing. *J. Geophys. Res.* **115**, D24312, doi:10.1029/2009JD013764.

Tesche, M., Ansmann, A., Müller, D., Althausen, D., Engelmann, R. and co-authors. 2009. Vertically resolved separation of dust and smoke over Cape Verde by using multiwavelength Raman and polarization lidars during Saharan Mineral Dust Experiment 2008. *J. Geophys. Res.* **114**, doi:10.1029/2009JD011862.

Tesche, M., Ansmann, A., Müller, D., Althausen, D., Mattis, I. and co-authors. 2011. Profiling of Saharan dust and biomass burning smoke with multiwavelength polarization Raman lidar at Cape Verde. *Tellus* **63B**, this issue.

Tulet, P., Mallet, M., Pont, V., Pelon, J. and Boone, A. 2008. The 7-13 March 2006 dust storm over West Africa: Generation, transport, and vertical stratification. *J. Geophys. Res.* **113**, 10.1029/2008JD009871.

van der Werf, G. R., Randerson, J. T., Giglio, L., Collatz, G. J., Mu, M. and co-authors. 2010. Global fire emissions and the contribution of deforestation, savanna, forest, agricultural, and peat fires (1997-2009). *Atmos. Chem. Phys.* **10**, 11707–11735, doi:10.5194/acp-10-11707-2010.

Wang, C. 2007. Impact of direct radiative forcing of black carbon aerosols on tropical convective precipitation. *Geophys. Res. Lett.* **34**, L05709, doi:10.1029/2006GL028416.

Washington, R., Todd, M. C., Middleton, N. J. and Goudie, A. S. 2003. Dust-storm source areas determined by the Total Ozone Monitoring Spectrometer and surface observations. *Ann. Assoc. Am. Geogr.* **93**, 297–313.

Wendisch, M., Müller, D., Schell, D. and Heintzenberg, J. 2001. An airborne spectral albedometer with active horizontal stabilization. *J. Atmos. Oceanic Technol.* **18**, 1856–1866.

Winker, D. M., Hunt, W. H. and McGill, M. J. 2007. Initial performance assessment of CALIOP. *Geophys. Res. Lett.* **107**(D21), 34, L19803, doi:10.1029/2007GL030135.

Wolke, R., Hellmuth, O., Knoth, O., Schröder, W., Heinrich, B. and co-authors. 2004. The chemistry-transport modeling system LM-MUSCAT: Description and CityDelta applications, In: *Air Pollution Modeling and Its Application XVI*, eds. C. Borrego and S. Incecik, Proceedings of twenty-sixth NATO/CCMS international technical meeting on air pollution modeling and its application, Kluver Academic/Plenum Publishers, New York.

Yoshioka, M., Mahowald, N., Conley, A. J., Collins, W. D., Fillmore, D. W. and co-authors. 2007. Impact of desert dust radiative forcing on Sahel precipitation: relative importance of dust compared to sea surface temperature variations, vegetation changes, and greenhouse gas warming. *J. Clim.* **20**(8), 1445–1467.

Yu, H. B., Liu, S. C. and Dickinson, R. E. 2002. Radiative effects of aerosols on the evolution of the atmospheric boundary layer. *J. Geophys. Res.* **107**(D12), doi:10.1029/2001JC000754.

Zhang, Y., Fu, R., Yu, H., Qian, Y., Dickinson, R., Silva Dias, M. A. F. and co-authors. 2009. Impact of biomass burning aerosol on the monsoon circulation transition over Amazonia. *Geophys. Res. Lett.* **36**, L10814, doi: 10.1029/2009GL037180.

Zhao, C., Liu, X., Leung, L. R. and Hagos, S. 2010. Radiative impact of mineral dust on monsoon precipitation variability over West Africa. *Atmos. Chem. Phys. Discuss.* **10**, 27 185–27 226, doi:10.5194/acpd-10-27185-2010.